

SPECTRAL STRUCTURE OF THE ALUMINUM DUST FLAME

Jorin Mamen, Samuel Goroshin, and Andrew Higgins
Mechanical Engineering, McGill University, Montreal Quebec, Canada H3A 2K6
samuel.goroshin@mcgill.ca

Introduction

The majority of practical applications of aluminum combustion such as solid rocket motors, dust explosions in industry, and chemical reactors involve combustion of dense dust suspensions of small particle sizes. The existing experimental and theoretical literature on the other hand, is mostly dedicated to the study of the combustion of isolated and relatively large particles. It has already been suggested in the literature that extrapolation of the results obtained with large single particles towards small single particles is questionable due to possible changes in the combustion mechanisms (*Yetter and Dryer, 2001*). The combustion of particles in a dense cloud where each particle is influenced by its neighbors through changes in bulk temperature, diminishing oxygen concentration, and changing concentration of intermediate gas species, is inherently transient and can be of very different physical nature from the combustion of an isolated single particle. Thus, the particles in a flame might burn with the formation of individual microflames around each particle (as has been observed with single particles) or collectively form a continuous flame sheet through merging of gaseous combustion zones. In the intermediate stage, combustion zones around several particles may merge, forming flame “clusters” whereas the rest may still burn as individuals as occurs during the combustion of liquid sprays (*Chiu, 2000*). However, because of several factors (i.e. the low volatility and very high boiling point of aluminum, formation of the intermediate gaseous aluminum oxides, and complex process of chemical condensation of these oxides into nanosized alumina particles) the structure of the flame in aluminum suspension is probably more complex than those in organic fuel sprays.

A laminar, Bunsen-type dust flame is a convenient way to study the structure of flame fronts in dense particle suspensions. It provides spatial separation of different stages of particle combustion, in contrast to moving flame fronts in tubes or transient combustion of the suspensions injected into hot gas, which often produce turbulent fronts that have very complex geometry. In our recent works we have used a Bunsen dust flame to investigate the dependence of burning velocity on dust and oxygen concentrations in fuel-rich aluminum dust clouds (*Goroshin et al., 1997*) and the effect of the nozzle geometry and flow characteristics on the measured burning velocity (*Goroshin et al., 2001*). The current paper presents an attempt to identify the combustion mechanism of aluminum particles in a dense dust suspension by spatially resolved emission spectroscopy of the Bunsen flame front.

Experimental set-up.

The details of the experimental set-up of the “dust burner” which permits stabilization of the Bunsen-type laminar aluminum flame are described elsewhere (*Goroshin et al., 1996, 1997*). This set-up allows observation of the aluminum flame at dust concentrations close to or exceeding the stoichiometric value in air. In the present work, the aluminum dust flame (see Fig. 2A) was stabilized above the conical nozzle with an exit diameter of about 20 mm. The schematic of the scanning spectral system that permits acquisition of the spatially resolved flame spectra is shown in Fig. 1 below.

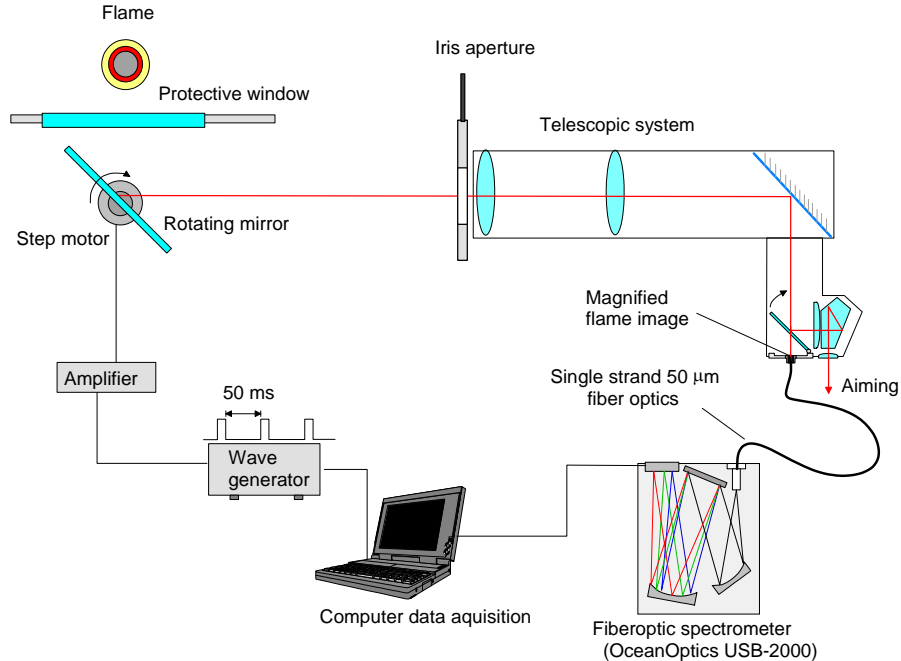


Figure 1 Schematics of the spectral scanning system.

A miniature fiber-optic spectrometer (USB-2000, OceanOptics Inc.) provides digital acquisition of the spectra in the wavelength range $\lambda = 400 - 1000$ nm using a 2048-element linear CCD array. The magnified ($\times 1.5$) image of the flame is obtained through the first surface aluminum mirror mounted on a step motor, telescopic system, and conventional Canon SLR camera with macro T-rings (see Fig. 1). The light from some chosen point on the flame image obtained on the film plane of the camera is transmitted to the spectrometer via a 50 micron diameter, 5 meter long single-strand optical fiber. The fiber aperture also plays the role of the spectrometer entrance slit. The estimated spectral resolution of the spectrometer is about 1.5 nm. To account for the non-uniform spectral sensitivity of the CCD sensor, a calibration was performed using a tungsten halogen light source (LS-1-CAL, Ocean Optics Inc.) with a known distribution of spectral emissivity.

The step motor is operated by an amplified signal from the square wave generator. The generator produces a preset number of square pulses of adjustable frequency and duration. The same signal also triggers the computer-based data acquisition system. A small delay of about 10 msec is introduced into the triggering line to stop spectral acquisition during the actual movement of the mirror. Though the technical characteristics of the spectrometer allows acquisition of about 70 spectra per second, this number at present was limited to about 20 per second due to the low speed of the computer USB digital interface. The spatial distance between acquisition points across the flame was about 250 microns. Thus, about 40 spatial points and correspondingly about 2 seconds were required to traverse the flame from the centerline to the periphery of the flame cone.

Experimental spectra and Abel deconvolution procedure.

An example of the spectra in the spectral range 400-900 nm acquired from five consecutive points close to the flame front is shown in Fig. 2B. Clearly defined molecular bands ($B^2\Sigma^+ \rightarrow X^2\Sigma^+$) of gaseous aluminum suboxide (AlO) and double line of sodium are the only recognizable gaseous emitters visible above the background of continuous spectra.

It is generally accepted (Bucher et al., 2000) that aluminum burns through a series of steps in which AlO is a key intermediate. AlO is an early product of aluminum combustion and during single particle combustion is quickly oxidized to AlO₂ and then to Al₂O₃ at several particle radiuses from the surface (Yetter and Dryer, 2001).

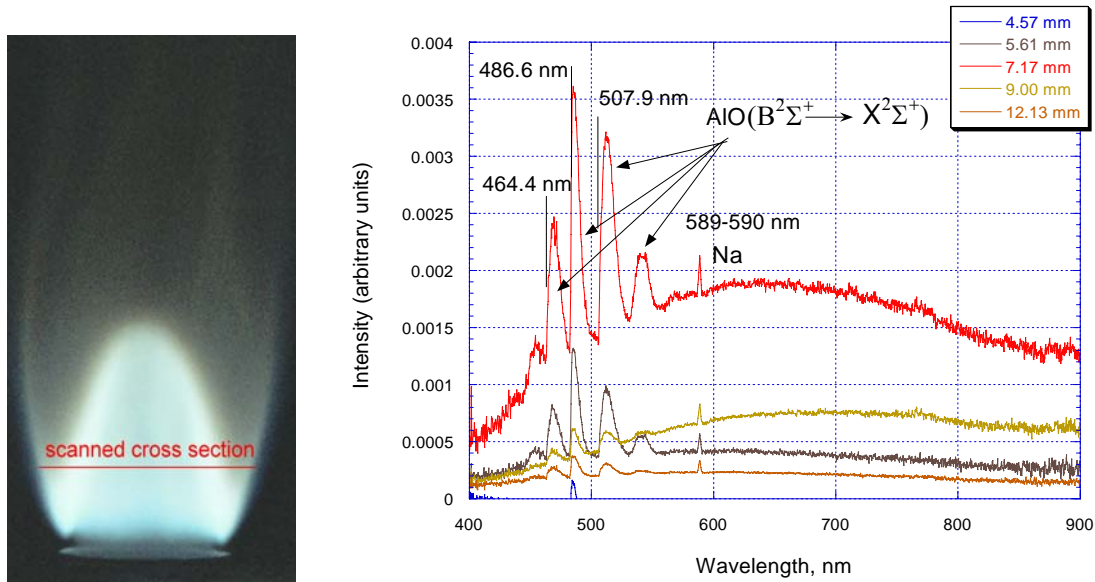


Figure 2 Photograph of the Bunsen-type aluminum dust flame and an example of spectra obtained at several distances from the flame border.

An example of the spatial distribution of light intensity at 570 nm is plotted in Fig. 3. For every recorded wavelength, the distribution (analogous to that shown in Fig. 3) was approximated by a 6th degree polynomial to smooth out noise. Since the raw data is a line-of-sight projection through a cylindrically symmetrical object, the data had to be deconvolved in order to extract the real radial distribution of relative light intensities. An Abel deconvolution transform using the “onion peeling” method (Dasch, 1992) was used.

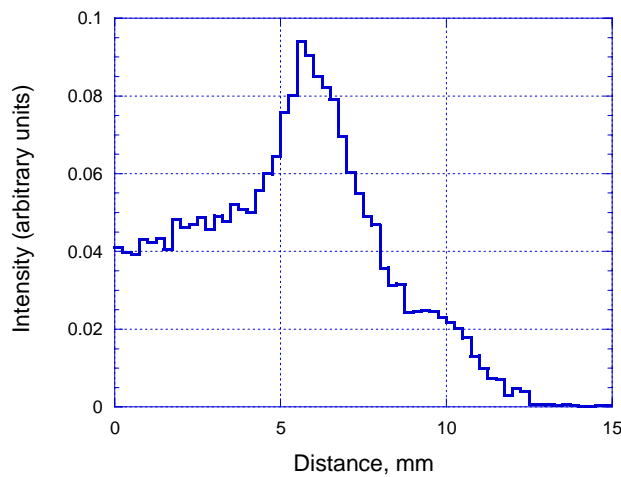


Figure 3 Dependence of the light intensity on distance at 570 nm (raw data).

The three-dimensional graphs illustrating spatial and spectral distributions (intensities plotted as a function of wavelength and flame radius) recovered by the Abel deconvolution are

shown in Fig. 4. The flame's inner boundary appears around 5.5 mm from the central axis. The second rise in intensity that is observed at the outer flame border indicates a weak diffusive flame front resulting from combustion of fuel-rich products from the inner flame with oxygen from surrounding air.

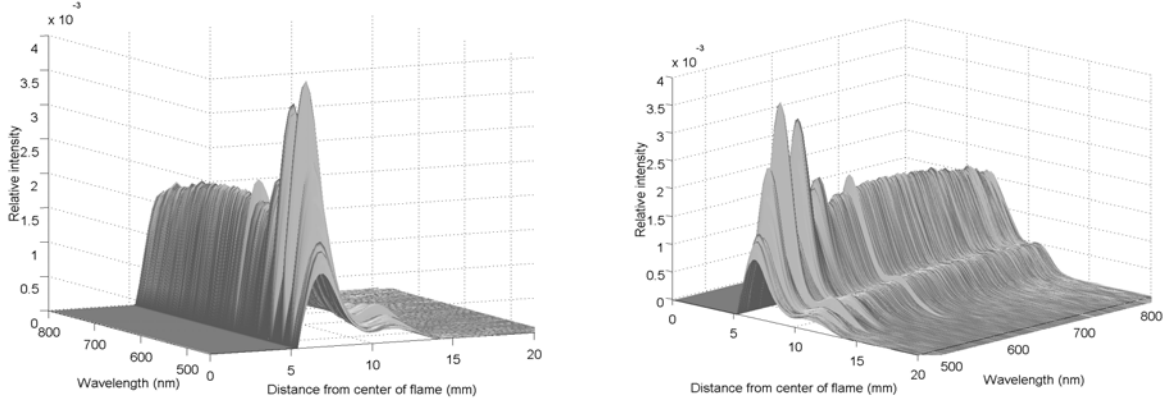


Figure 4 Spectral-spatial structure of the flame front after Abel deconvolution (A- inside view and B- outside view of the flame front).

Deriving temperatures from continuous spectra and from AlO molecular bands.

The obtained spectra were used to calculate radial temperature distributions from two different light emitters in the flame. The first temperature was from the solid particles (continuous part of the spectra) and the other from gas species (AlO bands).

The spectral distribution of the light intensity emitted by the condensed phase (solid or liquid particles) is described by the general Plank's law:

$$i_{\lambda,T} = \varepsilon(\lambda,T) \cdot 2\pi c_1 \lambda^{-5} [\exp(c_2/\lambda T) - 1]^{-1} \quad (1)$$

Here $\varepsilon(\lambda,T)$ is the spectral emissivity (arbitrary function) of the condensed light-emitting substance, $c_1 = 0.5954 \cdot 10^{-16} \text{ W} \cdot \text{m}^2$, and $c_2 = 1.4388 \cdot 10^{-2} \text{ m} \cdot \text{K}$. For so called "gray" emitters, $\varepsilon(\lambda,T)$ is considered to be independent on wavelength and the Plank law can be written in the next form, where the logarithm of spectral intensity is a linear function of $1/\lambda$, where the slope of the linear dependence is proportional to $1/T$:

$$\ln \left\{ \frac{i_{\lambda,T} \cdot \lambda^5}{\varepsilon(T)} \cdot 2\pi c_1 \right\} = c_2 / \lambda T \quad (2)$$

As can be seen in Fig. 5, the spectral light intensity plotted in accordance with expression (2) deviates considerably from a straight line, suggesting that condensed emitters in the flame are not gray. This could be expected, as the hottest sources of the continuum spectra in flame are submicron particles of aluminum oxide. The average particle size of aluminum oxide is comparable or smaller than the wavelength of light in the observed part of the spectrum (400-1000 nm). For such small aluminum oxide particles light absorption (and therefore emission) cross sections strongly decrease with wavelength (Plass, 1964). The best fit to linear dependence (2) was found with the assumption that emissivity of the condensed matter is inversely proportional to λ^2 , see Fig. 6.

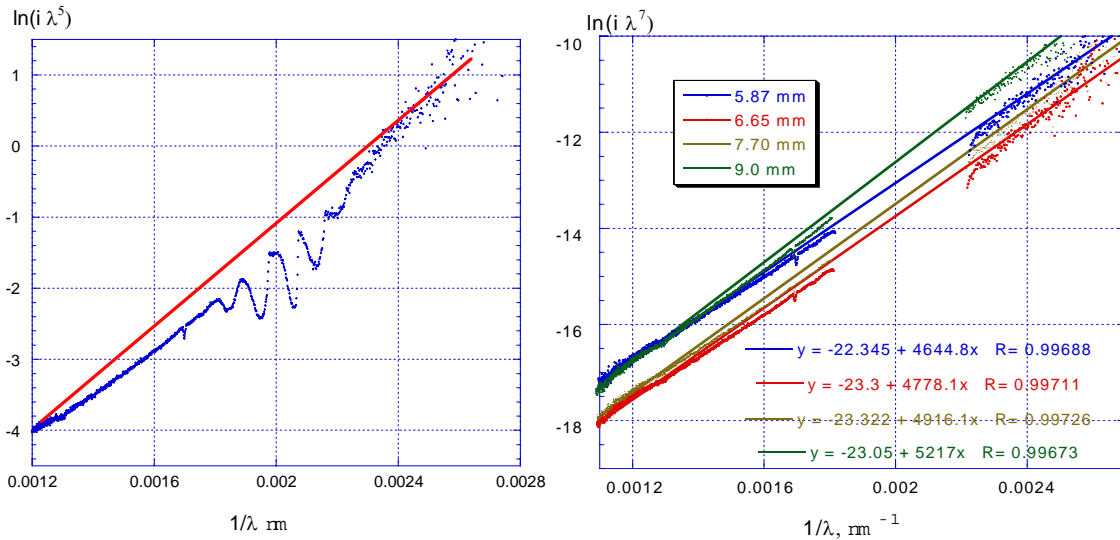


Figure 5 Illustration of the non-gray nature of the continuous spectra of the aluminum dust flame.

Figure 6 Linear fitting with the assumption that $\varepsilon(\lambda, T) \sim \lambda^{-2}$.

The spatial distribution of the temperature along the radius, derived from continuous spectra using raw scanning data is shown in Fig. 7A. The distribution from the processed data (after the Abel deconvolution) is shown in Fig. 7B.

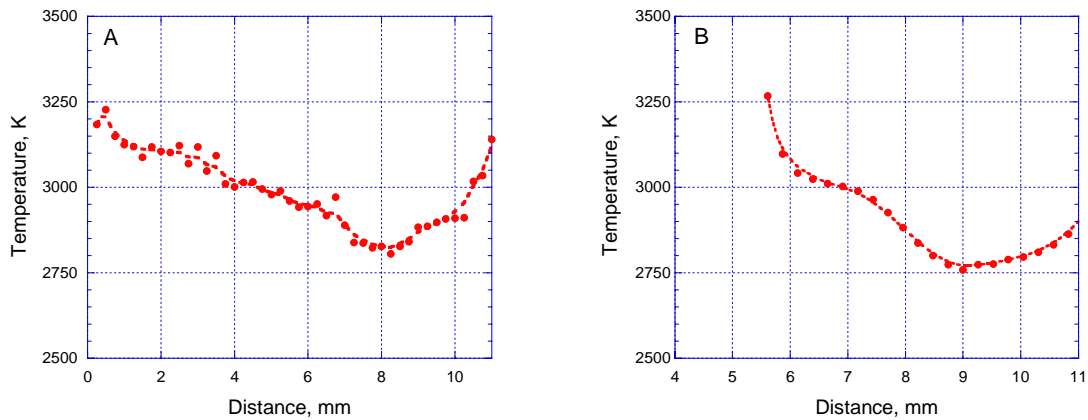


Figure 7 Spatial distribution of the temperature derived from continuous spectra using raw (A) and deconvolved (B) data.

As the Abel transform is a linear operator and does not modify the spectral distribution of light intensities, the range of the temperature change remains essentially the same before and after deconvolution. The maximum temperature of the continuum spectra is about 3250 K and coincides with the flame's inner boundary. The temperature decreases sharply over a distance of less than 1 mm, and is then followed by a gradual decrease to a minimum temperature of about 2750 K. The second rise in temperature that is observed at the outer flame border indicates a weak diffusive flame front resulting from fuel-rich products from the inner flame cone zone mixing with oxygen from surrounding air. The temperature distribution of AIO intermediate gaseous oxide was derived while assuming an optically thin source. The AIO temperature at each point was found by fitting theoretically calculated spectra to experimental data using AIO

$\Delta\nu = -1$ single band sequence which is the most sensitive to temperature¹. The fitting procedure is illustrated in Fig. 8.

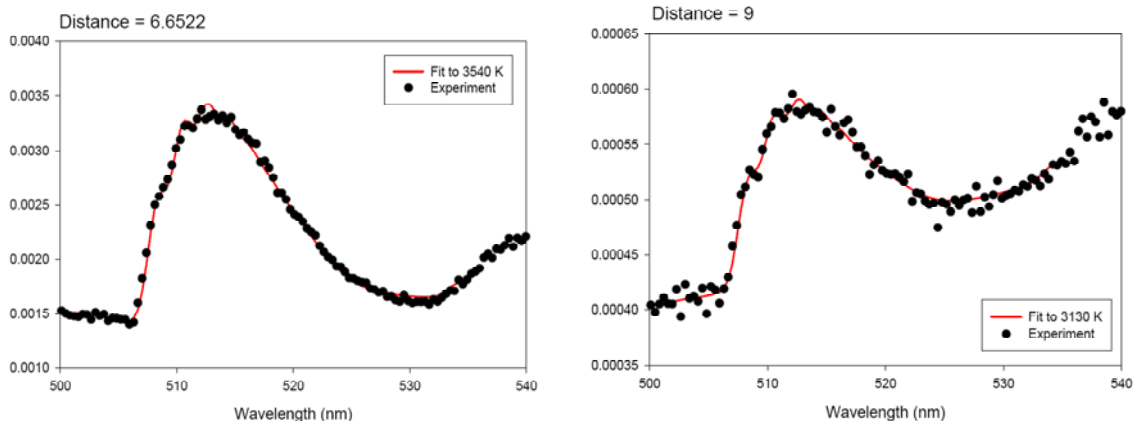


Figure 8 Fitting procedure of the theoretical calculations and experimental data for derivation of the temperature of AIO.

The spatial temperature distribution of AIO derived from deconvolved data is shown in Fig. 9 in comparison to the temperature distribution previously derived from the spectra of condensed emitters.

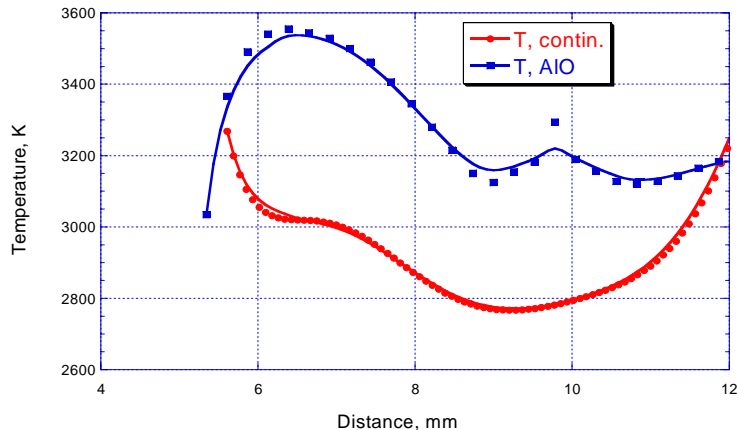


Figure 9 Spatial temperature distribution derived from continuous spectra and AIO molecular band.

Discussion

As can be seen from Fig. 9, the temperatures derived from AIO spectra are an average of 200 to 500 degrees higher than the temperature of continuum spectra. This fact however provides no firm ground for radical conclusions. The relatively low spectral resolution of the spectrometer used (about 1.6 nm) does not permit observation of the fine structure of AIO bands and leads to relatively large uncertainties in temperatures (up to several hundred degrees) derived from the band-shape fitting procedure described above (*Glumac et al., 2005*). More important is the observed difference in the character of temperature profiles derived from continuous and molecular spectra. The temperature of continuous spectra attains a maximum value at the beginning of the flame front and then falls rapidly, whereas the temperature of AIO reaches its

¹ This work was performed by Dr. Nick Glumac at University of Illinois at Urbana-Champaign.

maximum at some distance from the beginning of the flame front and then gradually decreases. The difference in the value and behavior of gaseous and solid temperatures is difficult to explain by simple non-equilibrium effects in the multi-phase media such as radiation heat loss etc. Most probably, these differences result from some kind of micro-diffusion flame structure that surrounds particles inside the bulk flame sheet (flame inside flame). The rapidly falling temperature of the continuous spectra is consistent with micro-diffusion flame behavior, whose temperature would rapidly decrease following depletion of the oxygen. In contrast, the rising temperature of gaseous aluminum monoxide is similar to the temperature profile that one would expect from a homogeneous gas flame. A peculiar combination of diffusively burning particles that produce aluminum monoxide and a bulk gaseous flame where this monoxide is later oxidized towards AlO_2 and eventually condenses to Al_2O_3 seems to be a plausible explanation for the observed temperature behavior. Future work planned by the authors will include calculation of the concentration profile of AlO in the flame, more accurate measurements of the AlO temperatures, and also the study of flames with different inert carrier gases (Ar, He). This is all expected to shed more light on the complex structure of aluminum dust flame.

Acknowledgments

Authors would like to acknowledge Dr. Niliga Nigam, Department of Mathematics and Statistics at McGill University in helping develop Abel deconvolution algorithm and are also thankful to Dr. Nick Glumac from University of Illinois at Urbana-Champaign for calculating AlO temperatures.

References

- Bucher, P. Ernst, L. Dryer, F.L. Yetter, R. A., and Parr, T.P. (2000), Detailed studies on the flame structure of aluminum particle combustion. V. Yang, T.B. Brill, and W.Z. Ren (Eds.) *Progress in Astronautics and Aeronautics Vol. 185: solid Propellant Chemistry, Combustion, and Motor Interior Ballistics*. AIAA, Reston, VA, pp. 689-722
- Chiu H.H. (2000) "Advantages and Challenges in Droplet Spray Combustion. I. Towards a Unified Theory of Droplet Aerochemistry" *Prog. in Energy and Comb. Sci.*, 26, pp. 383-416
- Yetter, R. A. and Dryer, F. L., (2001) "Metal Particle Combustion and Classification" in the book "*Microgravity Combustion*", Howard Ross ed, Academic Press, New York, pp. 419-473
- Dasch, C., (1992) "One-dimensional tomography: a comparison of Abel, onion-peeling and filtered backprojection methods", *Applied Optics*, Vol. 31, No. 8, pp. 1146-1152
- Glumac, N., Krier, H., Bazyn, T., Eyer, R. (2005) "Temperature Measurements of Aluminum Particles Burning on Carbon Dioxide" *Comb. Sci. and Tech.*, 177, Pp. 485-511
- Goroshin, S., Fomenko, I., and Lee, J.H.S. (1997), Burning Velocities in Fuel-Rich Aluminum Clouds, *Proc. Comb. Inst.* 26: 1961-1967.
- Goroshin, S., Kolbe, M., Lee, J.H.S. (2001) Burning Velocity Measurements in Aluminum-Air Suspensions Using Stabilized Dust Flames, *ICDERS 2001*, Seattle.
- Plass, G., N. "Mie Scattering and Absorption Cross Sections for Aluminum and Magnesium Oxide" *Applied Optics*, Vol. 3, No.7, pp. 867-872